

The Giant Herbig-Haro Flow HH 212 and Associated Star Formation

BO REIPURTH,¹ C.J. DAVIS,² JOHN BALLY,³ A.C. RAGA,⁴ B.P. BOWLER,⁵ T.R. GEBALLE,⁶ COLIN ASPIN,⁷ AND HSIN-FANG CHIANG⁸

¹*Institute for Astronomy, University of Hawaii at Manoa
640 N. Aohoku Place, Hilo, HI 96720, USA*

²*National Science Foundation, 2415 Eisenhower Ave, Alexandria, VA 22314, USA*

³*CASA, University of Colorado, Boulder, CO, USA*

⁴*Instituto de Ciencias Nucleares, UNAM, México*

⁵*McDonald Observatory and the Department of Astronomy, University of Texas at Austin, Austin, TX 78712, USA*

⁶*Gemini Observatory, 670 North Aohoku Place, Hilo HI 96720, USA*

⁷*Institute for Astronomy, University of Hawaii at Manoa
640 N. Aohoku Place, Hilo, HI 96720, USA*

⁸*National Center for Supercomputing Applications, Urbana, IL 61801, USA*

ABSTRACT

The bipolar jet HH 212, among the finest collimated jets known, has so far been detected only in near-infrared H₂ emission. Here we present deep optical images that show two of the major bow shocks weakly detected in optical [SII] emission, as expected for a bona fide Herbig-Haro jet. We present widefield H₂ images which reveal two more bow shocks located symmetrically around the source and along the main jet axis. Additionally, examination of Spitzer 4.5 μ m images reveals yet another bright bow shock further to the north along the jet axis; no corresponding bow shock is seen to the south. In total, the HH 212 flow has an extent of 1050 arcsec, corresponding to a projected dimension of 2.0 pc. HH 212 thus joins the growing group of parsec-scale Herbig-Haro jets. Proper motion measurements indicate a velocity of about 170 km/sec, highly symmetric around the source, with an uncertainty of ~ 30 km/sec, suggesting a probable age of the giant HH 212 flow of about 7000 yr. The jet is driven by a deeply embedded source, known as IRAS 05413–0104. We draw attention to a Spitzer near- and mid-infrared source, which we call IRS-B, located only 7'' from the driving source, towards the outskirts of the dense cloud core. Infrared photometry and spectroscopy suggests that IRS-B is a K-type star with a substantial infrared excess, except that for an extinction of $A_V = 44$ the star would have only a weak infrared excess, and so in principle it could be a K-giant at a distance of about 2 kpc.

Keywords: stars: formation — stars: low-mass — stars: protostars — stars: pre-main sequence

1. INTRODUCTION

Bipolar outflows are fundamental characteristics of young stars, and have been detected at all evolutionary stages from Class 0 to Class III. These outflows are detected in molecular, atomic, and ionized transitions, representing physical conditions from shock-heated fast-moving plasmas to slower and denser molecular gas entrained from the ambient medium. Outflows are important sources of feedback into the ambient medium in star forming regions and form part of the self-regulation

of star formation. The most dramatic manifestations of the outflow phenomenon are the Herbig-Haro jets, highly collimated high-velocity bipolar flows that emit mainly in Balmer lines, forbidden lines of [SII], [OII], [FeII], and molecular transitions of H₂ (for reviews see e.g. Reipurth & Bally 2001, Frank et al. 2014, and Bally 2016).

One of the finest collimated and highly symmetric jets known is HH 212, discovered by Zinnecker et al. (1998). It is located in the L1630 cloud complex in the tenuous 'gap' between the rich star forming regions NGC 2023/2024 to the southwest and NGC 2068/2071 to the northeast. Its distance is assumed to be ~ 400 pc (Anthony-Twarog 1982, Kounkel et al. 2017). The clos-

est region of star formation to HH 212 is the Ori B9 region to the southwest (see Figure 9 of Miettinen 2012). The driving source of HH 212 is IRAS 05413–0104, a Class 0 source embedded in a cloud core that is flattened and rotating perpendicular to the jet flow axis (Wiseman et al. 2001, Lee et al. 2006, 2014). The HH 212 jet has been observed in the infrared in the principal H_2 transition at $2.212\ \mu\text{m}$ by Davis et al. (2000), Smith et al. (2007), and Correia et al. (2009). From radial velocities and proper motions, the water masers are found to move along the jet axis, and Claussen et al. (1998) deduced that the outflow axis lies within 5° of the plane of the sky. The jet was studied in SiO by Takami et al. (2006), Codella et al. (2007), and Cabrit et al. (2007, 2012), and the associated molecular outflow has been studied in detail by Lee et al. (2000, 2006, 2007, 2008, 2015), Codella et al. (2014, 2016) and Leurini et al. (2016). ALMA observations have revealed an accretion disk (Bianchi et al. 2017, Lee et al. 2017, 2018a) and have been used to explore the jet launching region and an associated disk wind (Podio et al. 2015, Codella et al. 2016, Tabone et al. 2017, Sahu et al. 2018, Lee et al. 2018b).

The HH 212 driving source was detected in the millimeter continuum by Zinnecker et al. (1992) and Chini et al. (1997), and in the radio continuum at the VLA by Galván-Madrid et al. (2004). Recently Chen et al. (2013) found, using 1.3mm and $850\ \mu\text{m}$ interferometry, that it is a binary source, MMS-1 and 2, with a separation of $0.53 \pm 0.05''$, and they detected a very faint third source, MMS-3 at a separation of $1.2 \pm 0.1''$, and coincident with a source tentatively detected earlier at 1.4 mm by Codella et al. (2007). However, these two additional sources have not been detected in ALMA studies of the region, so the potential multiplicity of the source needs to be examined further.

In this paper, we show that parts of the jet are observable at optical wavelengths, and using widefield H_2 imaging we find new bow shocks at larger distances from the driving source, demonstrating that the HH 212 flow joins the ranks of the parsec-scale outflows. While the HH 212 star forming event is often seen as a case of isolated star formation, we also discuss evidence that several other young stars have formed in the immediate vicinity of the jet source. We also discuss the nature of a near-infrared source, located $7''$ from the driving source of HH 212, at a projected separation of 3000 AU .

2. OBSERVATIONS

The HH 212 region was observed with infrared imaging and photometry at UKIRT and Subaru, with infrared spectroscopy at Gemini, and with optical imag-

ing at the ESO New Technology Telescope, as described below.

HH 212 IRS-B was observed with GNIRS (Elias et al. 2006) at the Gemini-North 8m telescope on UT Jan 1, 2013 (program GN-2012B-Q-86) with a total on-source exposure time of 2 hr 40 min under photometric conditions. A 0.45 arcsec wide slit was used. Because of the nearby jet, the slit was not positioned in the parallactic angle, and the standard star, observed at the same airmass, was observed at the same position angle (23°).

The central part of HH 212 was observed at the 8m Subaru telescope on UT Jan 10, 2012 using IRCs (Tokunaga et al. 1998) and H ($1.64\ \mu\text{m}$) and K' ($2.15\ \mu\text{m}$) filters of the Mauna Kea Observatories system (Tokunaga et al. 2002). The conditions were photometric with a seeing around $0.9''$ at K' . The image scale is 52 mas per pixel and the field of view is $54''$ on a side. The total integration time was 200 and 50 seconds in the H and K' filters, respectively. A 10-point dithering was used to map the region. The airmass during the observations was around 1.1. The data reduction was done using the Image Reduction and Analysis Facility (IRAF), following standard procedures described in the IRCs cookbook. Following Connelley et al. (2008), aperture photometry was performed using IMEXAMINE in IRAF with five aperture sizes ($0.9''$, $1.2''$, $1.5''$, $1.8''$, and $2.1''$). The standard stars were measured in the same way and the magnitudes from the UKIRT Faint Standards (Leggett et al. 2006) were adopted to give magnitude estimates of the targets. The K magnitude from the standard catalogue is used as the standard K' magnitude. This is an acceptable approximation because the K and K' filters have similar bandwidth in the Mauna Kea Observatories Near-Infrared filter set. Also, the standard stars used are early A type stars which further mitigate the difference. Measurements using different aperture sizes and different standard stars are averaged and errors are estimated. Furthermore, a minimum photometric error is estimated by the standard deviation of the standard star photometry. For each target, the error is determined by the standard deviation of individual measurements using different standard stars and different aperture sizes. The two errors are combined by a Pythagorean sum to represent the overall photometric uncertainty. For airmass correction, we use the median extinction values from Krisciunas et al. (1987). The extinction coefficient value for the K -band is used for our K' observations. The error introduced by this is of the order of 0.001 mag in terms of airmass correction, and much smaller than the quoted errors.

HH 212 was observed with EMMI at the ESO New Technology Telescope (NTT) on February 6, 1995 using

a [SII] filter (ESO #655). The exposure time was 1800 sec.

A widefield near-infrared image of HH 212 was taken on February 14, 2010 through an H₂ filter ($\lambda \sim 2.1215$ micron, $\delta\lambda \sim 0.021$ micron) using the UKIRT Wide Field Camera WFCAM (Casali et al. 2007) in a seeing of 1.0 arcsec. Individual 60 sec exposures were repeated with a 5-point dither pattern and 2×2 micro-stepping (this yields a 0.2 arcsec pixel scale), resulting in a total integration time of 1200 sec. Comparison images were taken through a K-band filter ($\lambda \sim 2.20$ micron, $\delta\lambda \sim 0.34$ micron) on March 15, 2014 using the same camera, telescope and dither/microstep procedure, resulting in a total integration time of 200 sec. The seeing varied between 1.1 and 1.5 arcsec.

A second-epoch H₂ image was obtained on January 5, 2018 also using WFCAM on UKIRT in Directors Discretionary Time. On this occasion 40 sec exposures were repeated with a 9-point jitter and 2×2 micro-step pattern, resulting in a total integration time of 1440 sec. The seeing was about 0.9 arcsec on this occasion.

Reduction of all of the WFCAM data was performed by the Cambridge Astronomical Survey Unit (CASU). The pipeline processing and science archive are described in Irwin et al. (2004).

3. RESULTS

3.1. HH 212 Morphology from Infrared and Optical Images

The HH 212 jet known up to now is about 4 arcminutes in extent, corresponding to a projected length of 0.46 pc at the distance of 400 pc, and is well studied on those scales. However, many HH flows have much larger dimensions (e.g., Reipurth et al. 1997), and we have searched for further components along the flow axis. Figure 1 shows an image from the MHO Catalogue¹ obtained in the H₂ transition at $2.212 \mu\text{m}$. To the south, approximately along the well defined flow axis, a newly discovered large bow shock is seen, here labelled OS (for Outer-South)², it is very similar in morphology and size to the two major shocks at the ends of the hitherto known parts of HH 212. There is a slight change in orientation of about 4° in the line from the source to the apex of this new distant bow shock relative to the axis of the innermost jet knots. In fact, close examination shows a gradual change in orientation from the inner-

most to the outermost knots, suggesting precession of the flow axis. The displacement is towards the west.

We have also searched north along the flow axis, and here find a very faint diffuse knot along the precise same line through the source region and the new OS bow shock, but slightly closer to the source. The knot, which we label ON (for Outer-North), is very faint, and we have verified that it is pure H₂ emission by comparing to a broadband K-image. The displacement for this knot relative to the axis of the inner jet knots is to the east, as expected for a precessing flow axis. With these new shocks, the total projected extent of the HH 212 flow is now 12.6 arcminutes, which at 400 pc corresponds to 1.47 pc, so HH 212 joins the group of parsec-scale HH flows.

Finally, we have examined the available Spitzer IRAC-2 ($4.5 \mu\text{m}$) images obtained of this region. It is well known that many outflows emit in the $4.5 \mu\text{m}$ band, which often is depicted as green in multi-filter IRAC color images, and hence are dubbed 'Extended Green Objects' or EGOs (e.g. Cyganowski et al. 2008). Such objects, including the HH 212 jet, are well seen in the Spitzer $4.5 \mu\text{m}$ image, and the emission is believed to be mainly from the (0-0) S(9) line of H₂ at $4.69 \mu\text{m}$, possibly with additional CO vibrational emission (Takami et al. 2010). We have found yet another even more distant bow shock along the northern outflow lobe, see Figure 2. No corresponding bow shock is seen to the south. We dub this northern bow shock ON2. The total distance from ON2 to OS is 1050 arcsec, which at 400 pc corresponds to a projected separation of 2.0 pc. Takami et al. (2010) studied the inner region of the HH 212 jet in the Spitzer $4.5 \mu\text{m}$ and $8.0 \mu\text{m}$ filters, and showed an excellent correspondence with H₂. Thus, although the bright and large bow shock ON2 lies outside our UKIRT WFCAM field, we expect it to be emitting in H₂ (1-0) S(1) rovibrational emission at $2.12 \mu\text{m}$ as well.

Figure 10a shows an enlargement from the H₂ image, presenting the well studied inner parts of the HH 212 jet. The entire jet emits in molecular hydrogen, but since Herbig-Haro objects are defined in terms of optical emission lines (primarily H α and [SII]), upon its discovery a [SII] image was obtained by one of us (BR) with the ESO 3.5m NTT, where it was found that both of the main bow shocks of HH 212 are faintly visible through the screen of extinction that covers the jet. On this basis the jet complex was given the name HH 212. A new deeper optical image from the Subaru telescope is shown in Figure 10b, where the faint visible HH knots are marked with circles.

3.2. Proper Motions

¹ The MHO Catalogue can be found at <http://www.astro.ljmu.ac.uk/MHCat>, where HH 212 is listed as MHO 499 (Davis et al. 2010).

² This has independently been discovered by Mark McCaughrean (priv. comm.)

Proper motions were derived from our 2010 and 2018 UKIRT images obtained through an H_2 filter. The time difference is 2882 days. During this time the jet moved measurably, and we have used a wavelet convolution method to derive the proper motions; the method is described in Raga et al. (2017). Figure 4 shows the resulting velocity vectors and the values in km/sec are listed in Table 2. The motion along the jet axis is evident. While the error box on each individual vector is non-negligible, taken together the motion is well established. The X and Y values in Table 2 were measured with the jet oriented along the Y-axis. Given the very well defined flow axis, we interpret the $V(X)$ values perpendicular to the jet axis as the uncertainty of the measurements, yielding a value of 30 km/sec on individual velocities. The values along the jet-axis are assumed to be due to the physical motion of the knots, and we find a remarkable symmetry around the source, with identical values of the northern (171 km/sec) and southern jet (170 km/sec). Since the jet is oriented only about 5° from the plane of the sky this projected velocity also corresponds to the space motion of the jet. The motion of the new southern bow shock is around 180 km/sec, albeit with a much larger spread in $V(X)$ of 50 km/sec. However, the result suggests that the jet is not slowing down as it ploughs through the ambient medium, in contrast to the HH 34 giant jet complex, which shows a major deceleration from source to terminal shocks (Devine et al. 1997). The new most distant bow shock (ON2) is located outside our UKIRT images, and hence we have not obtained its proper motion.

Assuming a constant velocity of ~ 170 km/sec and a distance of 400 pc, the innermost pair of bright knots (NK1 and SK1) have ages of 75 yr, and the next pair of bright knots (NB1/2 and SB1/2) are 500 yr old. The last symmetric pair of bright shocks is NB3 and SB3, which are 1050 yr old. After that we see three more distant bright bow shocks, SB4 at 1550 yr, the new southern bow shock OS at 4300 yr and the most distant northern bow shock ON2 at 7000 yr. We thus see a progression of larger and larger intervals between the bow shocks as we move away from the source, and this is discussed further in Section 4.

3.3. Jet Opening Angle

Jets gradually expand as they leave their sources, and it has been shown that close to the source they expand sideways very rapidly, after which the expansion slows down and reaches a constant rate (e.g., Reipurth et al. 2000).

The opening angles of the finely collimated jets HH 1 and HH 34 have been measured accurately on HST im-

ages, and the half-opening angle for HH 1 is 1.3° and for HH 34 it is 0.4° (Reipurth et al. 2000, 2002). We have used archival HST NICMOS images³ to measure the opening angle for the HH 212 jet. Figure 5 shows the inner 30 arcsec of the jet around the source. Due to high obscuration, the innermost part of the jet is not visible even in these near-infrared images. At their widest, the well resolved bright inner knot pair NK1 and SK1 (using the nomenclature of Zinnecker et al. 1998), has a mean width of $1.56''$. This leads to a mean half-opening angle for this knot pair of $6.8 \pm 0.5^\circ$. With an approximate tangential velocity of 170 km s^{-1} the two knots were ejected from the source 73 yr ago. Under the assumption that the jet started within the innermost few AU of the star-disk system, this implies that the two knots have a mean radial expansion velocity of 20 km s^{-1} . In the internal working surface model of Raga et al. (1990), the jet knots are small working surfaces moving into a co-moving medium. The morphology of the knots NK1 and SK1 very much fit that interpretation. A working surface consists of an outer bow shock and an inner jet shock or Mach disk. In a rest frame moving with these two shocks, ambient material moves into the bow shock and jet gas moves into the Mach disk, leading to gas being expelled sideways and a consequent lateral expansion of the knot. It is difficult to compare this measurement with shock models, because the sideways ejection velocity is a function of several poorly known parameters, especially the cooling rate. Given that molecular hydrogen is highly excited in HH 212, and the $S(1)$ line of H_2 that we observe in HH 212 is excited in weak shocks, it follows that the lateral gas expulsion in the NK1/SK1 knots may be highly supersonic.

The opening angle of the HH 212 jet is significantly larger than measured for the HH 1 and 2 jets. One possible explanation for this may be that the HH 212 shocks are stronger, leading to a faster lateral expansion of the bow shock wings. We have also measured the width of the next two knots, NK2 and SK2, and find a half-opening angle of 2.3° , which is significantly less than for the NK1/SK1 pair, but still larger than for the HH 1 and HH 34 jets.

3.4. A New Wide Companion?

While studying the HH 212 jet on Spitzer IRAC images, we noticed a nearby source with a strong $8 \mu\text{m}$ flux, unlike any of the other numerous background stars in the region. We have studied this source further, and will below argue that this is possibly a new distant com-

³ Program 7368, PI: M. McCaughrean

ponent, here called IRS-B, in the Class 0 multiple system IRAS 05413—0104, or HH 212 MMS.

3.4.1. Photometry

Figure 6a,b shows images obtained in H- and K-filters of the innermost region of the HH 212 jet. In addition to multiple knots in the jet, three near-infrared sources are seen. IRS-B is marked, located at α_{2000} 05:43:51.2, δ_{2000} -01:02:47. The MMS source was detected at the VLA by Galván-Madrid et al. (2004) at α_{2000} 05:43:51.408 δ_{2000} -01:02:53.13. The projected separation of MMS and IRS-B is thus 6.9 arcsec. Assuming that a line between the two sources lies at an angle of 30° to the plane of the sky, then at the assumed distance of 400 pc the physical separation of the two sources is about 3000 AU.

We have imaged IRS-B with the IRCS at the Subaru 8m telescope in H and K' filters. The star is readily detectable in both filters, see Figure 6a,b, with $H = 19.20 \pm 0.10$ mag and $K' = 15.95 \pm 0.11$ mag. IRS-B is also detected in all the four IRAC bands of Spitzer, yielding $[3.6] = 14.01 \pm 0.14$, $[4.5] = 13.16 \pm 0.12$, $[5.8] = 12.67 \pm 0.12$, $[8] = 11.15 \pm 0.15$ mag.

Figure 6c shows the IRAC 8 μ m image, in which IRS-B is clearly visible. IRS-B is not seen in the 24 μ m MIPS image, possibly due to its proximity to the HH 212 driving source, which is also a likely reason it is not seen in the submm and mm images of Chen et al. (2013).

Figure 7 shows the available photometry of HH 212 IRS-B from 1.6 to 8 μ m as black circles. Using the reddening curves of Fitzpatrick (1999) with $A_V/E(B - V) = 3.1$, the observed photometry has been dereddened by an A_V of 15 mag (blue triangles), 30 mag (green squares) and 44 mag (red circles). Two blackbody curves of 4570 K and 3916 K, corresponding to K0 and M0 giants (van Belle et al. 1999) are shown fitted to the H-band fluxes; the arguments for choosing this spectral range are based on a near-infrared spectrum and are discussed in the next section.

If one plots the Spitzer IRAC photometry in color-color diagrams (e.g., Gutermuth et al. 2008), IRS-B falls in the region of Class II sources bordering on Class I sources. A potentially high extinction, however, complicates the interpretation, and we therefore proceed as follows.

An important question to ask is whether IRS-B has any infrared excess. The answer is made difficult by the lack of detections shortwards of the H-band. If we make the assumption that the shortest wavelength detection in the H-band represents the photosphere of the star, then we can fit the abovementioned black body curves at this wavelength. For low extinctions, IRS-B has a major infrared excess at all observed wavelengths. By

increasing the assumed extinction to $A_V = 44$ mag., it is possible to fit the H-band and the [3.6], [4.8], and [5.8] bands to the black body curves, but both the K-band and [8]-band fluxes indicate excess. If one increases the extinction to larger values while maintaining the assumption that the H-band flux is photospheric, then the IRAC band fluxes fall underneath the black body curves, which is evidently unphysical. Higher extinctions than $A_V = 44$ mag. are possible, but then imply a near-infrared excess in both H- and K-bands. We conclude that the available photometry implies that IRS-B has an infrared excess, which may be significant for either low or very high extinction, or more modest if the extinction is around $A_V = 44$ mag.

If IRS-B is associated with the HH 212 star forming region, then its luminosity would be roughly $0.5 L_\odot$ if it follows the red curve for $A_V=44$ mag in Figure 7, and less if the extinction is lower. This is consistent with a young low-mass star.

If IRS-B is *not* a young companion to HH 212-MMS, then what is it? Statistically the most likely background star would be a K-giant. Assuming an extinction of $A_V=44$, and ignoring the small observed infrared excess for this extinction value, we find that a K-giant at a distance of roughly 2 kpc could match the photometry. Unfortunately, IRS-B is not visible in the optical, so Gaia cannot help in distinguishing between these possibilities.

It follows that on the basis of photometry alone, we cannot decide conclusively whether IRS-B is young or not.

3.4.2. Spectroscopy

Figure 8 shows a near-infrared spectrum in the H- and K-bands of HH 212 IRS-B. As expected from the near-infrared photometry provided above, the spectrum is extremely red, with only a low S/N in the H-band, and no signal at all in the J-band. In the K-band, a photospheric spectrum is seen, with pronounced CO band-head absorption between 2.3 and 2.4 μ m, and weak Na I, Ca I, and Mg I lines. Also, a weak H_2 2.122 μ m emission is seen, but given the strong and extended H_2 emission from the nearby jet, we cannot exclude that this might result from incomplete sky subtraction.

To constrain the spectral type of HH 212 IRS-B, we compare the 2.13-2.43 μ m region of our K-band spectrum to the IRTF library of cool stars from Rayner (2009) and Cushing (2005). This region contains a wealth of absorption lines sensitive to both temperature and surface gravity. We make use of both dwarf templates and giant templates for this exercise since this range of gravities likely brackets that of IRS-B. Our raw

data are complicated by high reddening and possible excess emission, so for this comparison we first normalize both the science spectrum and IRTF templates by fitting and subtracting a fourth-order polynomial to the continuum in that region. Following the method outlined in Bowler et al. (2009), we optimally scale each template to HH 212 IRS-B by computing the scale factor that minimizes the resulting χ^2 value. The reduced χ^2 values exhibit broad minima between \approx G3 and K7 spectral types for both the giant and dwarf spectra.

Closer examination of the spectrum in Figure 8 suggests a spectral type of IRS-B between K0 and M0. The absence of any water vapor bands in the GNIRS spectrum suggests that a later spectral type than early M is unlikely. The spectrum shows no sign of the lines of Ca/Fe/Mg around 1.95-2.00 μ m which become increasingly strong through the K spectral type. Also, there is no trace of TiO bands, which are dominant in M-stars. Hence it appears that, due to the extreme reddening, the spectral type of IRS-B cannot be determined accurately, and can be only loosely constrained to between K0 and M0, with K5 as the best fit.

In summary, the evidence points to IRS B being a young star, but the possibility that it could be a background K-giant cannot be excluded.

3.5. An Edge-on Disk and a Class I source

While examining the UKIRT images, we noticed what appears to be an edge-on disk 2 1/2 arcmin to the southwest of the HH212 source, see Figure 9. This object, which is located at α_{2000} 5:43:45.41, δ_{2000} -1:04:55.5, is not detected by 2MASS nor by WISE, and we refer to it as IRS-C. Reflection nebulae are apparent on either side of the disk, as well as a central faint point-like object, which presumably is the illuminating embedded star. The obscuration can be traced for about 10 arcsec on either side of the source, corresponding to a width of about 8000 AU. This is far too large to be a physical disk, and is more likely to represent the shadow cast by a much smaller circumstellar disk on its surroundings (see Hodapp et al. 2004). There is also a nebulous star about 18 arcsec to the NE of the edge-on disk, identified as 2MASS J05434630-0104439 and classified as a young star from Spitzer photometry (Megeath et al. 2012). We here refer to this object as IRS-D. The 2MASS colors are very red, and this continues into the WISE wavelength range, with W1=12.67, W2=11.19, W3=7.32, and W4=3.07, where it is the dominant source (see Figure ??). When placed in a [3.4]–[4.6] vs [4.6]–[12] WISE diagram, it falls in the middle of the Class I protostar region (see Koenig et al. 2012). These two objects demonstrate that although the HH 212 source is separate from

the nearest star forming complex Orion B9, it is not a completely isolated star forming event.

4. DISCUSSION

In the following we offer some speculations on the origin of IRS B assuming it is a young star.

Giant HH flows provide insight into the accretion history of their driving sources. Reipurth (2000) suggested a scenario which accounts for all the characteristics of giant outflows in terms of the evolution of an unstable triple system.

The most common outcome of the collapse and fragmentation of a cloud core is not the formation of a single star, but rather a binary or a small multiple system. This has long been suspected on theoretical grounds (Larson 1972), but is increasingly supported by observations at many wavelengths (e.g., Chen et al. 2013; for reviews see Goodwin et al. 2007 and Reipurth et al. 2014). When more than two stars are bound together in a non-hierarchical fashion, their motions are chaotic and inevitably result in the decay of the system, which either disintegrates or is re-structured into a hierarchical configuration (e.g., Valtonen & Mikkola 1991). This typically occurs during the protostellar phase (Reipurth 2000), and numerical simulations show that ejected components often for a while remain tenuously bound in wide orbits. While protostars generally are deeply embedded, such orphaned protostars, as they are dubbed, can be flung to the outskirts or outside of their nascent cloud core, making them observable at near-infrared or even at optical wavelengths (Reipurth et al. 2010). The ejected member is normally the lowest-mass component, and if the ejection occurs early enough that the stellar embryo has not accumulated sufficient mass to eventually burn hydrogen, it will remain a brown dwarf in the absence of further mass growth (Reipurth & Clarke 2001). Observations have indeed shown that the fraction of distant companions to Class I protostellar sources decreases dramatically as these sources become more evolved (Connelley et al. 2008).

It is during close triple approaches that the stars can exchange energy and momentum, and one of the bodies can be flung out. Such close interactions lead to massive accretion and outflow events, creating the large bow shocks seen at the extremities of giant HH flows. The remaining binary will have a highly eccentric orbit, and so when the two companions have their first periastron passage, their disks collide and another accretion/outflow event takes place. Due to such viscous interactions, the binary may slowly spiral in while becoming less eccentric, causing further and more closely spaced bow shocks.

In this picture, IRS-B would be an orphaned protostar residing at the edge of the HH 212 cloud core. This requires that the driving source of HH 212 is a binary. As noted earlier, the companion detected by Chen et al. (2013) is in doubt. However, such a binary would be so close that it would be hard to detect. If we assume that the hypothetical binary has a total system mass of $1 M_{\odot}$ and a period of 58 years, which is the time it would take the two innermost knots (NK1 and SK1 in the nomenclature of Lee et al. 2007) to reach the positions of the next pair of knots (NK2 and SK2) then we can derive a binary semimajor axis of 15 AU, which at the distance to HH 212 corresponds to 0.04 arcsec, assuming no projection effects. Such a companion would thus not be detected in currently available data.

If IRS-B is associated with the HH 212 region, then it is interesting to ask whether it is bound to the putative MMS binary, or it is escaping. And if it is bound, is it a stable or unstable system? In a major set of numerical simulations of triple systems, Reipurth & Mikkola (2012) calculated the ratios of stable, unstable, and disrupted triple systems as a function of projected separation. For a projected separation of about 3000 AU and an age of 1 Myr, it was found that only about 5% were unbound, while about 25% were stable triples, and about 70% were unstable triples. At first glance this would seem to contradict the fact that about 50% of all triple systems break apart during the protostellar phase. This is certainly true, but those escaping bodies have already moved much further away from their protostellar brethren. Only about 5% of unbound companions would still have a relatively small projected separation of around 3000 AU. While we are not able with current techniques to observationally determine whether IRS-B is bound or not, on a statistical basis we can state with some confidence that it is highly likely that IRS-B is still bound to the MMS binary, but only tenuously, and during one of the coming periastron passages, the system is likely to break apart, releasing IRS-B into a slow, gentle escape.

If IRS-B is indeed young, then the most interesting aspect of the star is that it is at all observable at near-IR wavelengths, even though it must have a very young age similar to the Class 0 source IRAS 05413-0104. Such newly born protostars are generally so deeply embedded that they are not observable at short wavelengths, but here we may have the opportunity to witness the stellar part of a very young protostar, thanks to its ejection from the deep interior of its cloud core. Because of its possible extreme youth, IRS-B should be located high up on its Hayashi track, and should therefore in principle be significantly more luminous than later in its evolution.

However, if it was ejected due to stellar triple dynamics, it would have lost some or much of its disk and envelope, leaving mostly the star itself to produce its luminosity. It will eventually appear in the optical as a late-type T Tauri star.

5. CONCLUSIONS

We have studied the region of the HH 212 bipolar jet and have obtained the following results:

1. The HH 212 bipolar jet is highly obscured and is visible mainly in molecular hydrogen transitions, but deep optical images show that the northern and southern bow shocks are optically visible.

2. We have discovered new distant bow shocks along the well defined flow axis of HH 212, increasing the size of the jet complex to ~ 2.0 pc and increasing the dynamical age of the system by a factor of more than 4.

3. We have measured the proper motions of the HH 212 jet complex, and for the inner highly symmetric pairs of knots we find a velocity of 170 km/sec with an uncertainty of about 30 km/sec. The new southern giant bow shock moves with the same velocity, suggesting that the jet is not slowing down as the flow penetrates the ambient medium. Since the angle of the HH 212 flow to the plane of the sky is only 5° the above velocity then equals the space velocity of the flow. For this velocity, the age of the giant HH 212 system is 7000 yr.

4. A Spitzer-detected near- and mid-infrared source has been noted $7''$ from the HH 212 source. The source shows an infrared excess for all extinction values, but it is minimal for $A_V=44$ mag. A H- and K-band spectrum shows a highly reddened K-type spectrum. If a background star it would be a K-giant at a distance of about 2 kpc. But the near- and mid-infrared photometry is also consistent with an embedded Class II source. We cannot distinguish between these two possibilities, but note that if IRS-B is associated with the HH 212 cloud core, then it is likely an orphaned protostar which – due to three-body interactions – has become detectable at near-infrared wavelengths. If so, the statistical analysis by Reipurth & Mikkola (2012) indicates that there is only a 5% chance that HH 212 IRS-B is currently escaping, but there is a 70% chance that it is presently only so tenuously bound that it will break loose when it dives into the cloud core during one of its coming periastron passages around the central protostars.

5. The HH 212 star forming event is located in a tenuous area of the L1630 cloud where the nearest star formation is in the Ori B9 region further to the southwest. We have shown that the HH 212 source is not so isolated, but has at least one Class I and one Class II object adjacent to it.

We thank the referee, Pat Hartigan, for helpful suggestions, and Tom Megeath for comments on the paper. We are grateful to Watson Varricatt and Tom Kerr for obtaining the UKIRT second-epoch image of HH 212 through Director’s Discretionary Time. UKIRT is owned by the University of Hawaii (UH) and operated by the UH Institute for Astronomy; operations are enabled through the cooperation of the East Asian Observatory. When some of the data reported here were acquired, UKIRT was operated by the Joint Astronomy Centre on behalf of the Science and Technology Facilities Council of the U.K. This project was supported by the Gemini Observatory, which is operated by the Association of Universities for Research in Astronomy, Inc., on behalf of the international Gemini partnership of Argentina, Brazil, Canada, Chile, and the US. Based in part on data collected at the Subaru Telescope, which is operated by the National Astronomical Observatory of Japan (NAOJ). and on observations

collected with the NTT at the European Organisation for Astronomical Research in the Southern Hemisphere. We acknowledge use of IRAC and MIPS data from the Spitzer Science Center. This research has made use of the SIMBAD database, operated at CDS, Strasbourg, France, and of NASA’s Astrophysics Data System Bibliographic Services, and of ESASky, developed by the ESAC Science Data Centre (ESDC) team and maintained alongside other ESA science mission’s archives at ESA’s European Space Astronomy Centre (ESAC, Madrid, Spain). This material is based upon work supported by the National Aeronautics and Space Administration through the NASA Astrobiology Institute under Cooperative Agreement No. NNA09DA77A issued through the Office of Space Science.

Facilities: UKIRT(WFCAM), Gemini-North(GNIRS), Subaru(IRCS), ESO-NTT(EMMI)

REFERENCES

- Anthony-Twarog, B.J. 1982, *AJ*, 87, 1213
- Bally, J. 2016, *Ann. Rev. Astron. Astrophys.*, 54, 491
- Bianchi, E., Codella, C., Ceccarelli, C. et al. 2017, *A&A*, 606, L7
- Cabrit, S., Codella, C., Gueth, F., Nisini, B., Gusdorf, A., Dougados, C., & Bacciotti, F. 2007, *A&A*, 468, L29
- Cabrit, S., Codella, C., Gueth, F., Gusdorf, A. 2012, *A&A*, 548, L2
- Casali M., Adamson A., Alves de Oliveira C., et al., 2007, *A&A*, 467, 777
- Chen, X., Arce, H.G., Zhang, Q. et al. 2013, *ApJ*, 768:A110
- Chini, R., Reipurth, B., Sievers, A., Ward-Thompson, D., Haslam, C.G.T., Kreysa, E., & Lemke, R. 1997, *A&A*, 325, 542
- Claussen, M.J., Marvel, K.B., Wootten, A., & Wilking, B.A. 1998, *ApJ*, 507, L79
- Codella, C., Cabrit, S., Cesaroni, R., Bacciotti, F., Lefloch, B., & McCaughrean, M. 2007, *A&A*, 462, L53
- Codella, C., Cabrit, S., Gueth, F. et al. 2014, *A&A*, 568:L5
- Codella, C., Ceccarelli, C., Cabrit, S. et al. 2016, *A&A*, 586, L3
- Connelley, M.S., Reipurth, B., & Tokunaga, A.T. 2008, *AJ*, 135, 2496
- Correia, S., Zinnecker, H., Ridgway, S.T., & McCaughrean, M.J. 2009, *A&A*, 505, 673
- Cyganowski, C.J., Whitney, B.A., Holden, E. et al. 2008, *AJ*, 136, 2391
- Davis, C.J., Berndsen, A., Smith, M.D., Chrysostomou, A. & Hobson, J. 2000, *MNRAS*, 314, 241
- Davis, C.J., Gell, R., Khanzadyan, T., Smith, M.D., Jenness, T. 2010, *A&A*, 511, 24
- Devine, D., Bally, J., Reipurth, B., Heathcote, S. 1997, *AJ*, 114, 2095
- Elias, J.H., Joyce, R.R., Liang, M. et al. 2006, *SPIE*, 6269, 62694C
- Fitzpatrick, E.L. 1999, *PASP*, 111, 63
- Frank, A., Ray, T.P., Cabrit, S. et al. 2014, in *Protostars and Planets VI*, eds. H. Beuther et al., Univ. of Arizona Press, p. 541
- Galván-Madrid, R., Avila, R., & Rodríguez, L.F. 2004, *Rev. Mex. Astron. Astrofis.* 40, 31
- Goodwin, S.P., Kroupa, P., Goodman, A., Burkert, A. 2007, in *Protostars and Planets V*, ed. B. Reipurth, D. Jewitt, & K. Keil (Tucson, AZ; Univ. Arizona Press), 133
- Gutermuth, R.A., Myers, P.C., Megeath, S.T. et al. 2008, *ApJ*, 674, 336
- Hodapp, K.W., Walker, C.H., Reipurth, B. et al. 2004, *ApJ*, 601, L79
- Irwin M. J., Lewis J., Hodgkin S., et al., 2004, in *Optimizing Scientific Return for Astronomy through Information Technologies*, eds. P. J. Quinn & A. Bridger, *Proc. SPIE*, 5493, 411
- Koenig, X.P., Leisawitz, D.T., Benford, D.J. et al. 2012, *ApJ*, 744, 130
- Kounkel, M., Hartmann, L., Loinard, L. et al. 2017, *ApJ*, 834, A142
- Krisciunas, K., Sinton, W., Tholen, K. et al. 1987, *PASP*, 99,887

- Larson, R.B. 1972, *MNRAS*, 156, 437
- Lee, C.-F., Mundy, L.G., Reipurth, B., Ostriker, E.C., & Stone, J.M. 2000, *ApJ*, 542, 925
- Lee, C.-F., Ho, P.T.P., Beuther, H., Bourke, T.L., Zhang, Q., Hirano, N., & Shang, H. 2006, *ApJ*, 639, 292
- Lee, C.-F., Ho, P.T.P., Hirano, N., Beuther, H., Bourke, T.L., Shang, H., & Zhang, Q. 2007, *ApJ*, 659, 499
- Lee, C.-F., Ho, P.T.P., Bourke, T.L., Hirano, N., Shang, H., & Zhang, Q. 2008, *ApJ*, 685, 1026
- Lee, C.-F., Hirano, N., Zhang, Q., Shang, H., Ho, P., Krasnopolsky, R. 2014, *ApJ*, 786:A114
- Lee, C.-F., Hirano, N., Zhang, Q., Shang, H., Ho, P.T.P., Mizuno, Y. 2015, *ApJ*, 805: A186
- Lee, C.-F., Li, Z.-Y., Ho, P.T.P. et al. 2017a, *ApJ*, 843, A27
- Lee, C.-F., Li, Z.-Y., Ho, P.T.P. et al. 2017b, *Science Advances*, 3:e1602935
- Lee, C.-F., Li, Z.-Y., Ching, T.-C. et al. 2018a, *ApJ*, 854, A56
- Lee, C.-F., Li, Z.-Y., Codella, C. et al. 2018b, *ApJ*, 856, A14
- Leggett, S.K., Currie, M.J., Varricatt, W.P. et al. 2006, *MNRAS*, 373, 781
- Leurini, S., Codella, C., Cabrit, S. et al. 2016, *A&A*, 595, L4
- Megeath, S.T., Gutermuth, R., Muzerolle, J. et al. 2012, *AJ*, 144:A192
- Miettinen, O. 2012, *A&A*, 545:A3
- Podio, L., Codella, C., Gueth, F. et al. 2015, *A&A*, 581, A85
- Raga, A.C., Cantó, J., Binette, L., Calvet, N. 1990, *ApJ*, 364, 601
- Raga, A.C., Reipurth, B., Esquivel, A. et al. 2017, *Rev. Mex. Astron. Astrofis.*, 53, 485
- Rayner, J.T., Cushing, M.C., Vacca, W.D. 2009, *ApJS*, 185, 289
- Reipurth, B. 2000, *AJ*, 120, 3177
- Reipurth, B. & Bally, J. 2001, *Ann. Rev. Astron. Astrophys.*, 39, 403
- Reipurth, B. & Clarke, C.J. 2001, *AJ*, 122, 432
- Reipurth, B. & Mikkola, S. 2012, *Nature*, 492, 221
- Reipurth, B., Bally, J., Devine, D. 1997, *AJ*, 114, 2708
- Reipurth, B., Heathcote, S., Yu, K.C. et al. 2000, *ApJ*, 534, 317
- Reipurth, B., Heathcote, S., Morse, J. et al. 2002, *AJ*, 123, 362
- Reipurth, B., Mikkola, S., Connelley, M., & Valtonen, M. 2010, *ApJ*, 725, L56
- Reipurth, B., Clarke, C.J., Boss, A.P., Goodwin, S.P., Rodriguez, L.F., Stassun, K.G., Tokovinin, A., & Zinnecker, H. 2014, in *Protostars and Planets VI*, eds. H. Beuther et al., (Tucson, AZ; Univ. Arizona Press), p.267
- Sahu, D., Minh, Y.C., Lee, C.-F. et al. 2018, *MNRAS*, 475, 5322
- Smith, M.D., O'Connell, B., & Davis, C.J. 2007, *A&A*, 466, 565
- Tabone, B., Cabrit, S., Bianchi, E. et al. 2017, *A&A*, 607, L6
- Takami, M., Takakuwa, S., Momose, M., Hayashi, M., Davis, C.J., Pyo, T.-S., Nishikawa, T., & Kohno, K. 2006, *PASJ*, 58, 563
- Takami, M., Karr, J.L., Koh, H., Chen, H.-H., & Lee, H.-T. 2010, *ApJ* 720, 2010
- Tokunaga, A.T., Kobayashi, N., Bell, J. et al. 1998, in *SPIE Conf Ser.*, ed. A.M. Fowler, vol. 3354, 512
- Tokunaga, A.T., Simons, D.A., & Vacca, W.D. 2002, *PASP*, 114, 180
- Umbreit, S., Spurzem, R., Henning, Th., Klahr, H., Mikkola, S. 2011, *ApJ*, 743:A106
- Valtonen, M.J. & Mikkola, S. 1991, *ARA&A*, 29, 9
- van Belle, G.T., Lane, B.F., Thompson, R.R. et al. 1999, *AJ*, 117, 521
- Wiseman, J., Wootten, A., Zinnecker, H., & McCaughrean, M. 2001, *ApJ*, 550, L87
- Zinnecker, H., Bastien, P., Arcoragi, J.-P., Yorke, H. W. 1992, *A&A*, 265, 726
- Zinnecker, H., McCaughrean, M., & Rayner, J. 1998, *Nature*, 394, 862

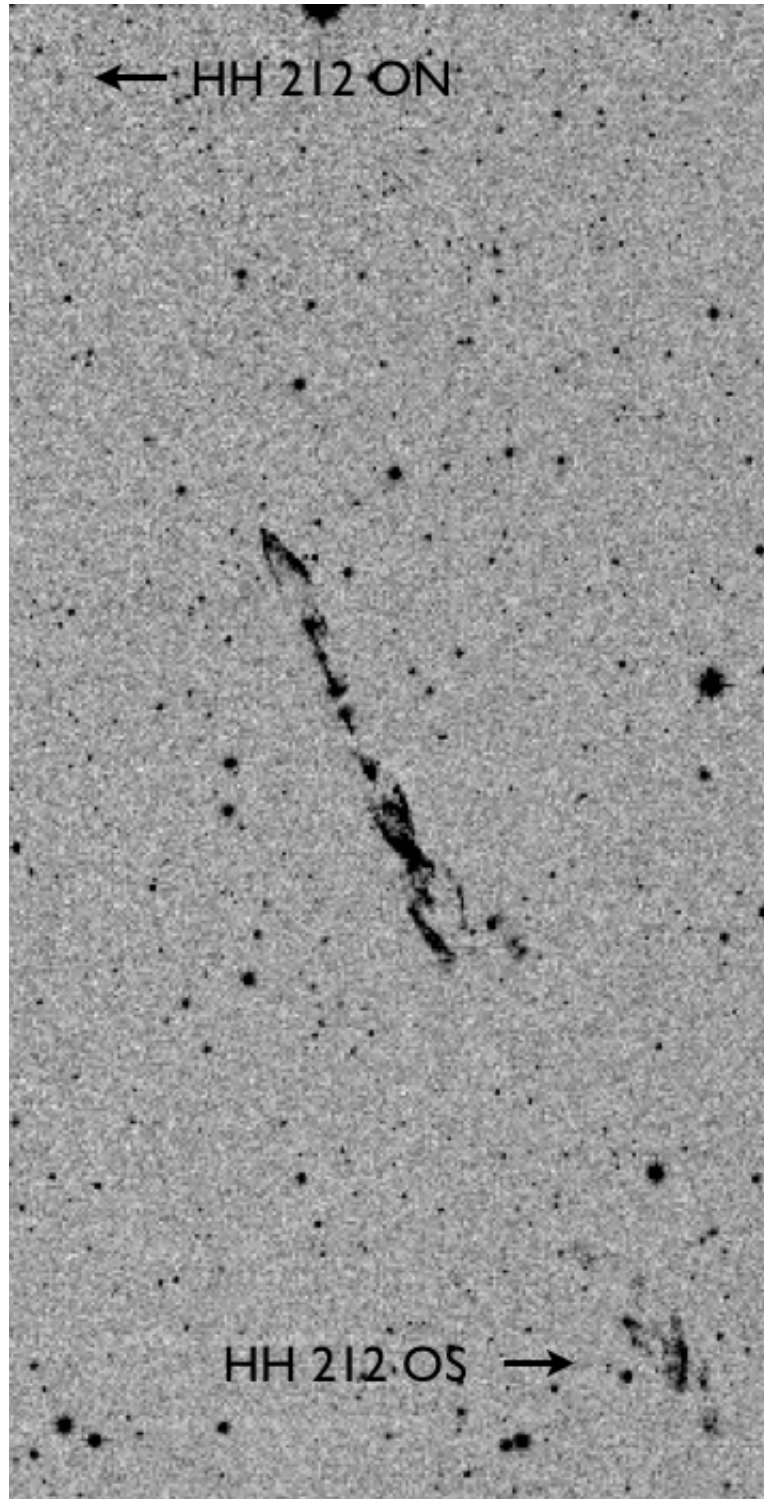


Figure 1. A molecular hydrogen image of the parsec-scale HH 212 flow obtained with WFCAM at UKIRT. North is up and east is left, and the vertical extent of the image is about 12 arcminutes.

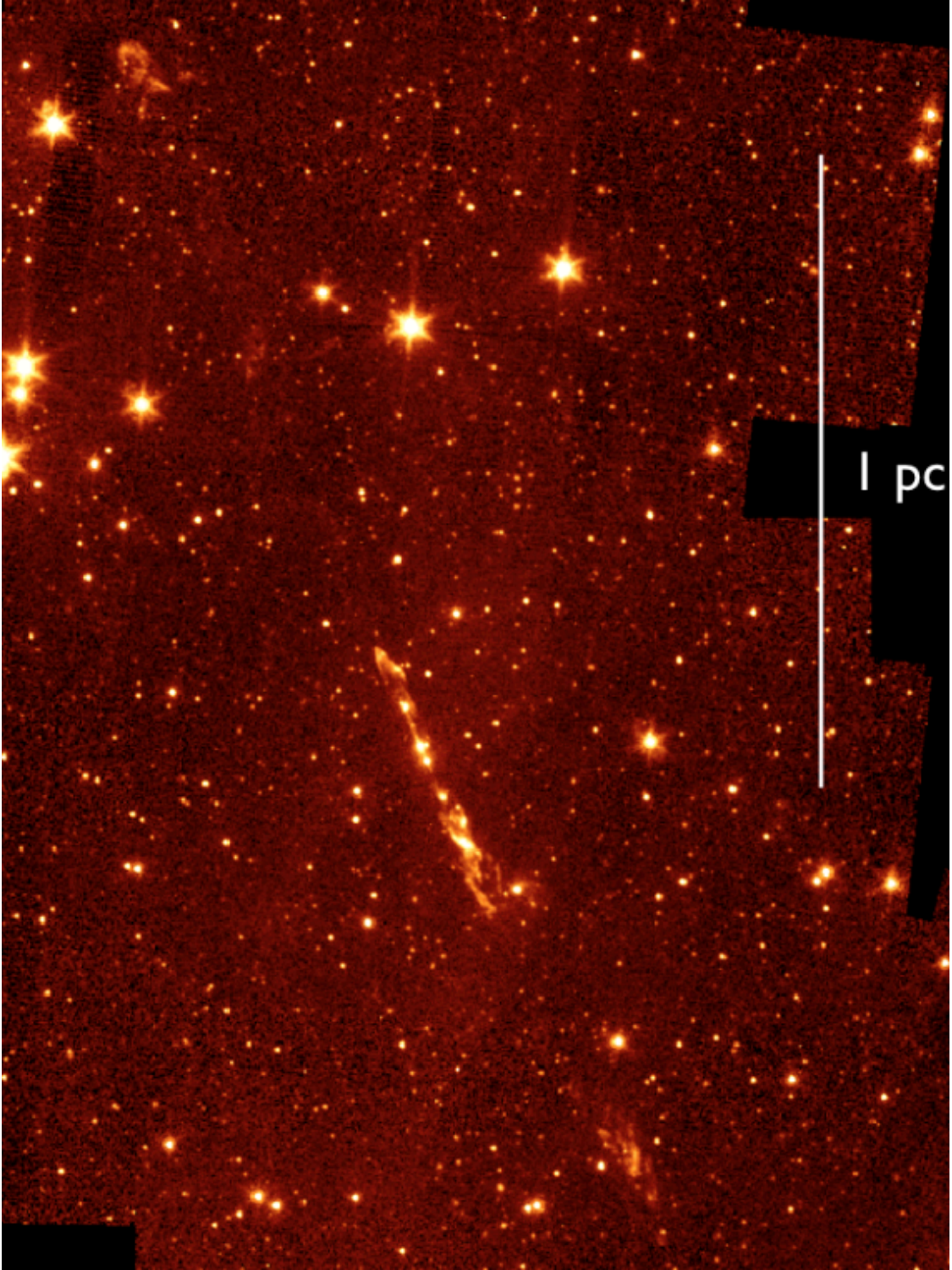


Figure 2. A Spitzer wide field Channel 2 image ($4.5\ \mu\text{m}$) of the HH 212 flow. All near-infrared components are seen, as well as a large bow shock outside the near-infrared WFCAM field. The total extent of the HH 212 is thus 1050 arcsec, corresponding to projected dimensions of 2.0 pc.

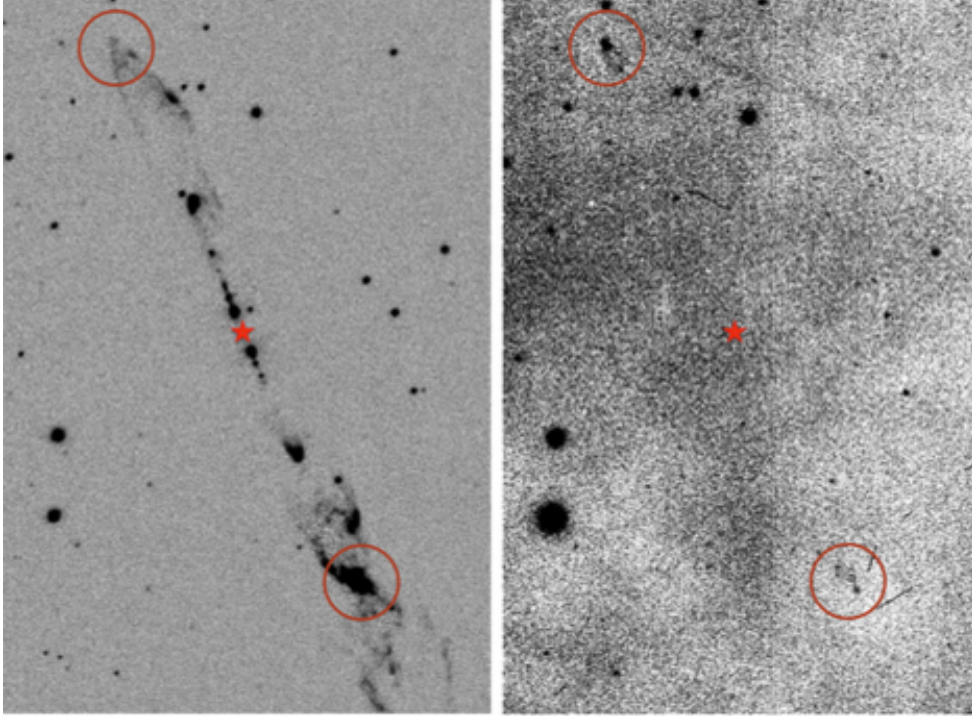


Figure 3. (a): H_2 $2.12\ \mu\text{m}$ image of the HH 212 jet from UKIRT. The embedded Class 0 driving source is marked with an asterisk. (b): $[SII]$ image of the approximate same region from the Subaru 8m telescope; the faint optical HH objects are marked by circles. Both images have north up and east left, and the vertical extent is about 4.5 arcminutes.

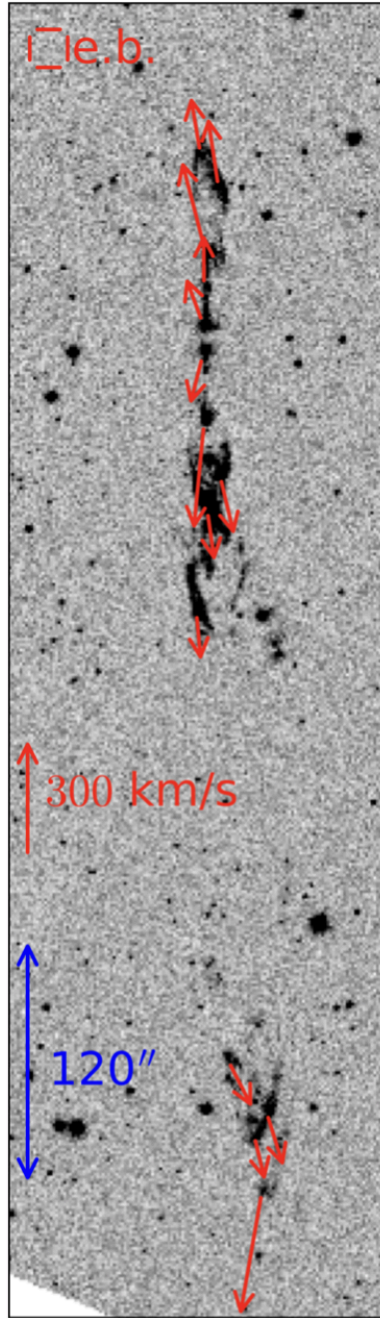


Figure 4. *Proper motions of the HH 212 knots. A typical error box is indicated in the upper left corner.*

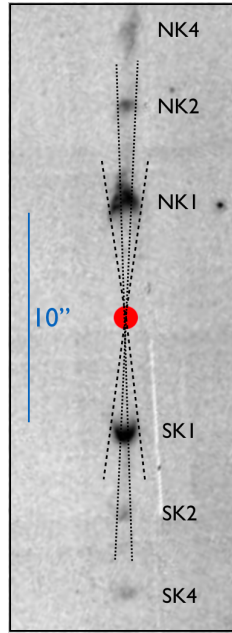


Figure 5. The innermost part of the HH 212 jet is seen here in an HST NICMOS H_2 image. The opening angle of the jet as measured for the first and the second pairs of knots is indicated.

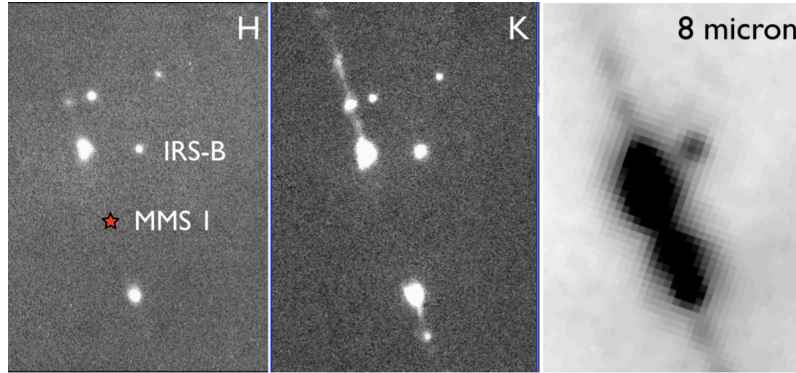


Figure 6. A mosaic of H- and K-band images of the center of the HH 212 flow taken with the Subaru 8m telescope, and an 8 μm image from Spitzer. IRS-B is marked, 7'' from the location of MMS. [fig:HKimage] North is up and east is left.

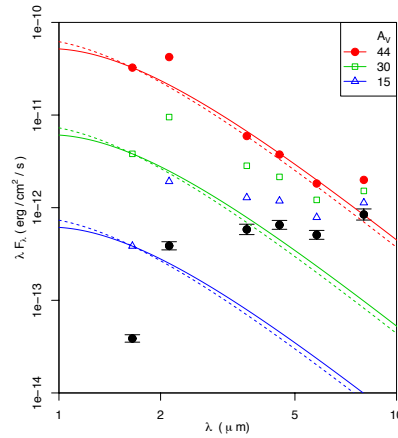


Figure 7. Available photometry of HH 212 IRS-B from 1.6 to 8 μm is plotted as black circles, the surrounding lines indicate the photometric uncertainty. The blue triangles, green squares and red circles show the same photometry de-reddened by $A_V = 15, 30$, and 44 magnitudes. Two black body curves for 3916 K (solid curve) and 4570 K (dashed curve) are fitted to the shortest wavelength photometric point for all three de-reddened data sets; these temperatures correspond to M0 and K0 giants.

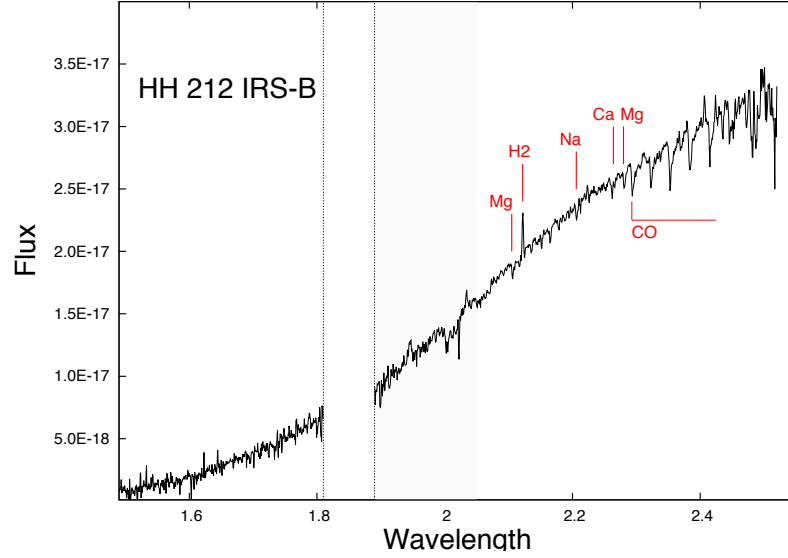


Figure 8. A GNIRS spectrum of HH 212 IRS-B from Gemini-North. Spectral features are indicated. The spectral region from 1.81 to 1.89 μm (between dotted lines) with strong atmospheric absorption (transmission $< 20\%$) has been removed, while the region from 1.89 to 2.05 μm with moderate atmospheric absorption (transmission $< 80\%$) is indicated by grey shading.

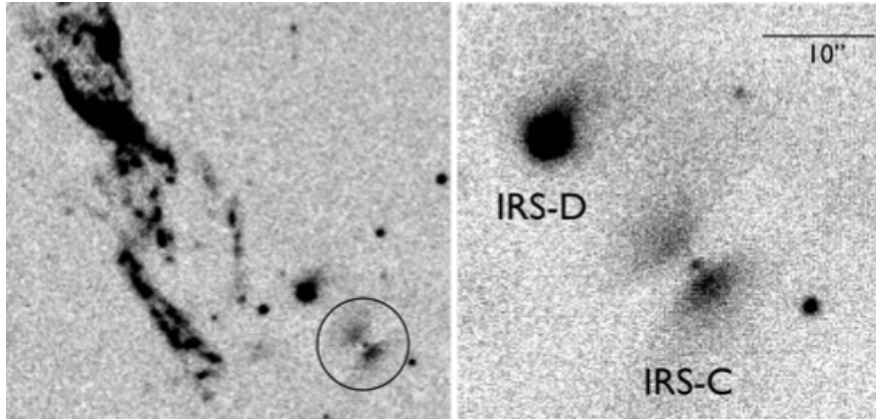


Figure 9. (a): An enlargement from the molecular hydrogen image in Figure 10a showing a small edge-on disk (encircled). The central star is faintly detected, and here called IRS-C. This new source is not detected by 2MASS or WISE, but is bright in a Herschel 250 μm image. (b) A K-band image of a region $\sim 38 \times 40$ arcsec showing the edge-on disk and its illuminating source IRS C. The star 18 arcsec to the NE is nebulous, and so apparently also young. It is here called IRS-D. North is up and east is left.

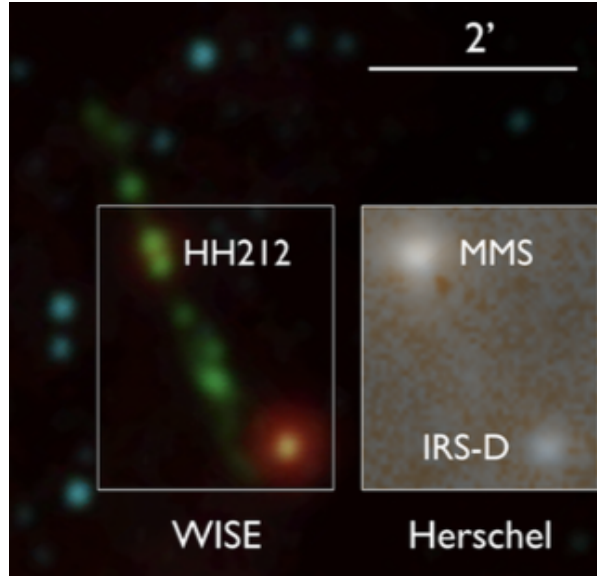


Figure 10. The HH 212 jet is seen in this WISE color image (blue 3.4 μm , green 4.6 μm , red 22 μm) together with the 2MASS source J05434630-0104439 (IRS-D) which is very bright at mid-infrared wavelengths. The framed region contains the two protostars MMS and IRS-D, and the insert to the right shows the same region as observed by Herschel at 70/160 μm . It is seen that the Class 0 source MMS is only visible at far-infrared wavelengths with Herschel, where it dominates the Class I source IRS-D that in turn dominates at near- and mid-infrared wavelengths. North is up and east is left.

Table 1. Positions of New Bow Shocks^a

| Bow Shock | α_{2000} | δ_{2000} | Source |
|-----------|-----------------|-----------------|---------|
| OS | 5:43:39.9 | -01:08:20 | UKIRT |
| ON | 5:44:00.8 | -00:57:42 | UKIRT |
| ON2 | 5:44:06.6 | -00:53:40 | Spitzer |

Table 2. Proper Motions^a

| Object ^b | ΔX^c | ΔY^c | $V(X)^d$ | $V(Y)^d$ |
|---------------------|--------------|--------------|----------|----------|
| NB3 | -1.2 | 86.6 | -27. | 157. |
| NB3 | 7.3 | 70.8 | -28. | 186. |
| NB1/2 | 1.3 | 40.3 | -61. | 236. |
| NK7 | 0.3 | 24.1 | 0. | 147. |
| NK1 | 0.0 | 6.8 | -48. | 129. |
| SK1 | 0.0 | -6.8 | -35. | -138. |
| SB1/2 | 0.5 | -38.7 | -27. | -273. |
| SB3a | 7.7 | -63.5 | 38. | -161. |
| SB3b | 1.8 | -79.5 | 20. | -143. |
| SB4 | -3.3 | -127.5 | 13. | -137. |
| OSa | 11.3 | -338.5 | 68. | -132. |
| OSb | 29.5 | -362.8 | 47. | -150. |
| OSc | 23.8 | -373.7 | 31. | -129. |
| OSd | 27.8 | -400.4 | -55. | -312. |

NOTE— *a*: Errors in individual velocities are ± 45 km/sec. *b*: Knot identifications starting with S or K are from Lee et al. (2007), and starting with O are from this paper. *c*: The x,y coordinates are measured in arcsecs from the source along (Y) and across (X) the outflow axis (positive Y to the N and positive X to the W.) *d*: Velocities are in km/sec assuming a distance of 400 pc.